

Final Report: 9/2/10

Experimental Design and Multi-scale Modeling of Self-Assembled Nanostructures for Hydrogen Generation and Utilization

DOT Program at the University of Vermont

Principal Investigators:

Walter Varhue

Darren Hitt

Yves Dubief

This Project was notified on March 8, 2007 that it was successful in securing funds from the US DOT Program supporting the development of Hydrogen as an Energy Source for Transportation.

The work on the hydrogen production portion of this project started soon after that day as it was already an active research area in our laboratory and this effort continues today with the hopes of securing future financial support. An SEM image of the RuO₂ nanorods is shown in Figure 1.0 below.

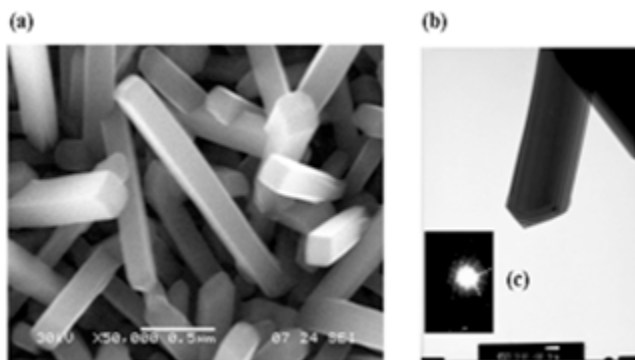


Figure 1. (a) SEM image of square RuO₂ nanorods grown on a Si substrate. (b) TEM scan of an individual nanorod, showing an atomically sharp pyramid tip. (c) Diffraction pattern indicates crystallinity.

The most significant results of the current research investigation can be listed as the following:

1. The RuO₂ nanorods have the remarkable property of strongly absorbing IR radiation, and the equally remarkable ability to not radiate IR radiation to its surroundings.
2. The presence/or the ability of a substrate material to form an oxide layer significantly influences to ability of that substrate to form RuO₂ nanorods.
3. The principal reason for the enhanced catalytic ability of the nanorods is associated with the increased interfacial area that it forms with an aqueous

solution and not the nanorod's shape which was thought to alter the electric field in the vicinity of the structures edges.

4. The presence of a Pt film or Pt containing quantum dots dramatically affects the hydrogen producing ability of these engineered nanorods materials.

Each of these four significant results are presently involved in some stage of dissemination through publication in a referred journal. In this report we summarize and discuss the scientific details and significance of each of these results.

1. Melting Nanorods

In an experimental investigation, we discovered that the material we had grown (nanorods of RuO₂ coated nanorod on a Si substrate surface) were melting at a substrate temperature of only 180 °C. This was remarkable as the melting temperature of the RuO₂ material is close to 1200 °C in bulk form. Upon SEM analysis of the heated RuO₂ nanorods, see figure 2 a and b, it was observed that the nanorods melted at only 180 °C, not completely to the puddle stage, but clearly visible as a loss of surface definition, and bending of the once straight rods.

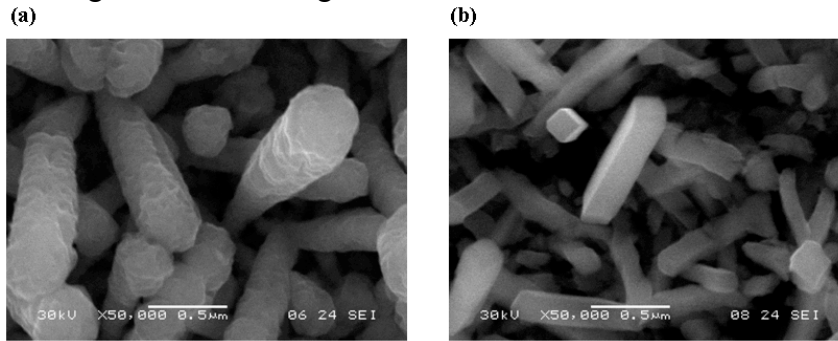


Figure 2. SEM images of 165 nm wide RuO₂ nanorods post anneal. Nanorods were grown on a Si substrate and (a) mounted to a stainless steel platen which was heated to 760 °C (substrate temperature was measured to be 700 °C) and (b) suspended 2 cm above a stainless steel platen which was heated to 760 °C (Si substrate temperature measured to be 180 °C).

The proposed explanation for this observation was that the conducting RuO₂ square nanorods are absorbing infrared radiation strongly as a result of the surface plasmon resonance,[1] SPR, from a heated stainless steel platen which was emitting a broad spectrum of IR radiation peaked at 2980 nm. The electronic plasmon disturbance on the surface of the nanorods was then coupled to phonons or lattice vibrations in the RuO₂ nanorods, thus raising their temperature.[2]

If the RuO₂ nanorods could emit black body radiation to their surroundings, this would peak just prior to melting at a temperature of 1200 °C, and by Wien's Displacement Law, correspond to peak intensity wavelength of 1730 nm. The emission or black body radiation or IR radiation from the nanorods has been predicted by Ding *et al.*[3] to be low however:

$$P_{radiation} = \int_0^{\infty} \sigma_{absorption} n(\omega, T) d\omega \quad (1)$$

with $n(\omega, T) = \text{Planck Function and}$

$$\sigma_{\text{absorption}} = \pi a^2 k_0 \ln \varepsilon$$

where a is effective nanorod diameter

$k_0 =$ wave vector (small at long wavelengths)

$\ln \varepsilon =$ imaginary permittivity (small at long wavelengths)

The nanorod material thus has no ability to emit black body infrared radiation to its environment, yet continues to absorb IR radiation via the SPR. The temperature of the nanorods continues to increase and they eventually melt at close to 1200 °C. These results were written into a journal publication and will appear in an upcoming issue of the *Nanotechnology*.

Armed with these results we proposed an investigation to the gas phase thermally enhanced electrolysis of water. This would be accomplished with the aid of a nano-material which would act as a chemical catalyst reducing the required activation energy, an electrode producing a high field region and as a platform that can be raised to an elevated temperature with the absorption of infrared radiation.

2. *Substrate Surface Required for Nanorod Growth*

The majority of previous discussions involved the growth of RuO₂ nanorods on a Si wafer substrate surface. The electrolysis of water for the production of hydrogen can be effectively accomplished in either basic or acidic aqueous solutions. The chemistry is such that the RuO₂ nanorods are vulnerable to chemical attack in acidic solutions, and the Si substrates are vulnerable to attack in a basic solution. To avoid this difficulty, it would be preferred to expand the list of acceptable substrates for the growth of RuO₂ nanorods. In Progress a previous report some result were given of work performed on the growth of RuO₂ nanorod structures on stainless steel substrate surfaces. In that earlier work it was concluded that surface roughness was preventing the formation of the nanorods. Some success was obtained by growing the nanorods on a mirror polished stainless steel substrate surface, see Figure 3. below.

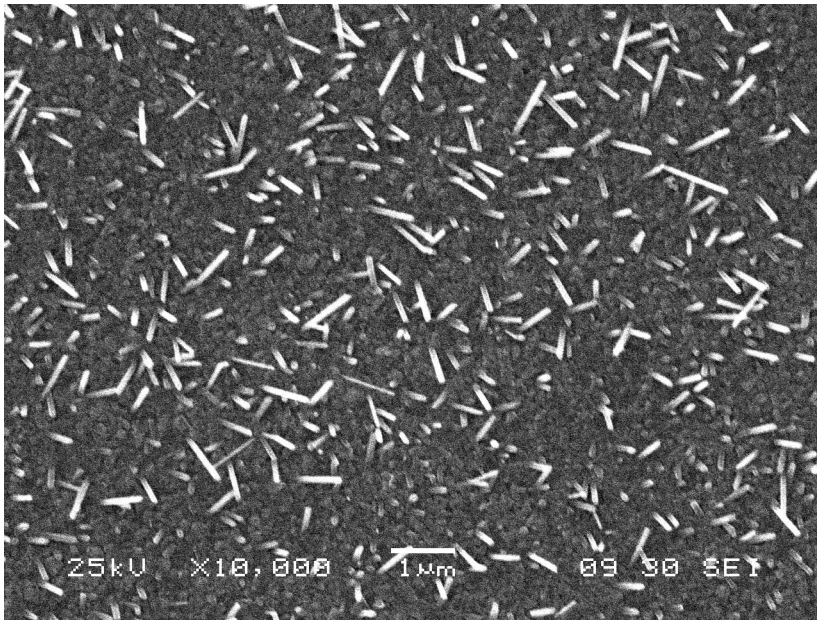


Figure 3. Growth on a polished stainless steel substrate surface.

The nanorods density shown in the micrograph picture above is less than half of that obtained on the Si wafer substrate. This result, and a reconsideration of previous results including growth on: Al coated Si, and borosilicate glass, it was postulated that it was the chemical nature of the substrate that determine successful growth of the nanorods. With this hypothesis it was decided to attempt the growth of the nanorods on a surface which was assured to be involved in a stable oxide coating. The Al substrate is known to contain a stable coating of Al_2O_3 . The material tried was that of Ti metallurgical foils. A SEM micrograph of this growth process can be found in Figure 4. below.

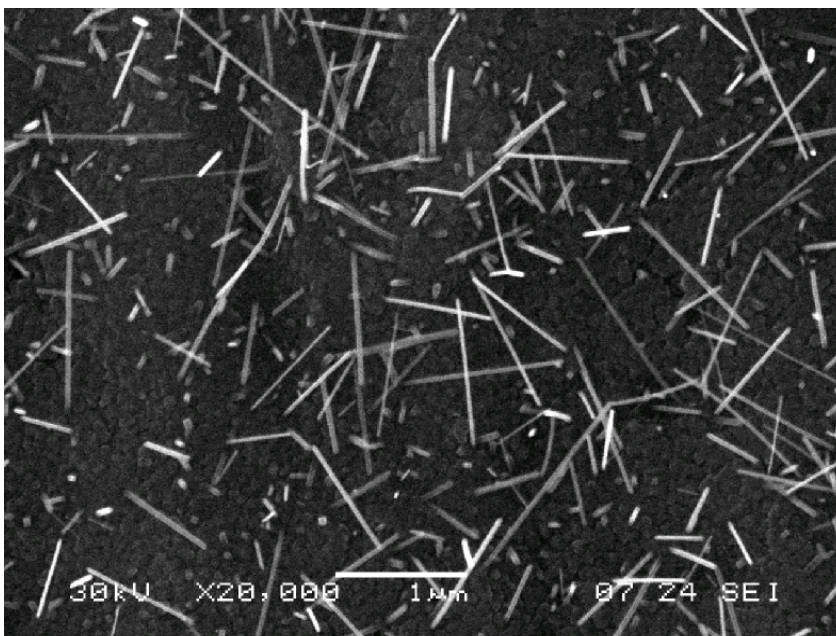


Figure 4. Growth of RuO₂ nanorods on a Ti metal foil.

This is a significant result as the assumed TiO₂ film is very thin (~ 1-2 nm) with a measured electrical resistance of about 1-5 Ohms. The chemical resistance of Ti and TiO₂ are legendary.

3. *Enhanced Catalytic Activity Due to Increased Interfacial Surface Area*

The electrolysis measure was performed in a custom made cell similar to the sketched in Figure 5.0. Relative to a Calomel reference cell, the electrical potential applied at the cathode was decreased until a voltage sufficient for current flow was reached. The anode in all cases was a Pt wire, 140 mm long, and 0.25 mm in diameter.

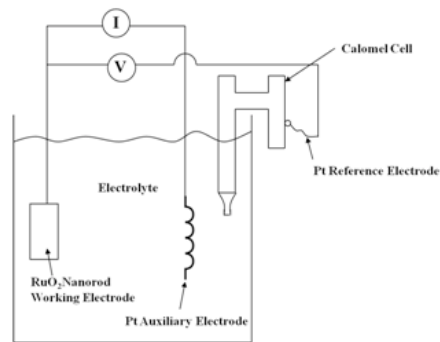


Figure 5. Sketch of experimental set-up. A 140 mm long, 0.25mm diameter Pt anode was used for all measurements and a Calomel reference cell was employed to provide a standard potential.

The production rate of H₂ per unit area of flat cathode surface was assumed to be directly proportional to the current density supplied to the cathode.

The measured J-V curves were observed to depend on the electrolyte concentration, and material used to construct the cathode electrodes. The work reported herein used an electrolyte of a 10 % solution of KOH in water. An example of the current density plotted as a function of the potential applied between the cathode electrode and the Calomel reference electrode is shown in Fig. 6. The anode in all cases was a piece of Pt wire. The current density measured was highest for the Pt (cathode) and otherwise was found to vary with substrate used to construct the nanorod coated cathodes, in the following order: Si, Al/Si, and Ti. The proposed reason for this variation is the resistance associated with the native oxide film that is assumed to be present on the cathode substrate surface prior to and during the growth of the RuO₂ nanorods. It is presumed that cathodes constructed of RuO₂ NR deposited on a Ti substrate would represent a preferred choice of materials, in terms of durability for manufactured cathodes.

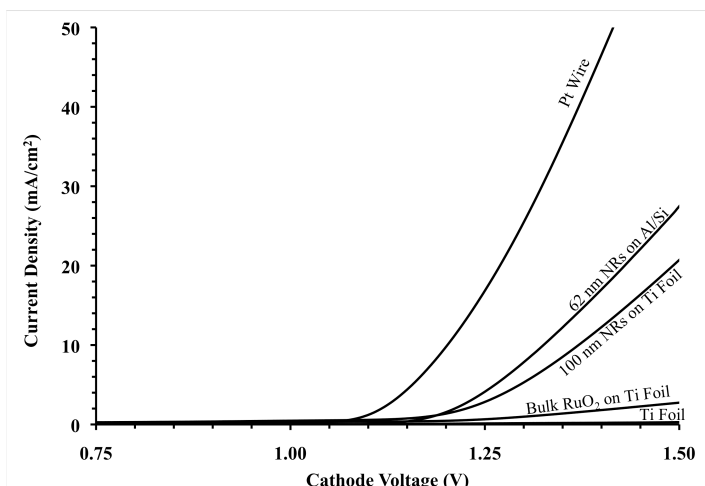


Figure 6. Electrical characterization of RuO₂ nanorods grown on various substrates. A 10% KOH solution was used as the electrolyte and a Pt wire was used as the anode. The cathode voltage is reported relative to the calomel reference electrode.

It is traditional to plot the current density versus the overvoltage for the electrode-electrolyte system that is used. The cathode over voltage (η_c) is defined as the experimentally applied potential, minus the theoretical potential value given by the Gibbs' Free Energy for the reaction ($2\text{H}^+ + 2\text{e}^- \rightarrow \text{H}_2(\text{g})$) under standard conditions ($E_{\text{cell}}^0 = 0.0 \text{ V}$), the correction supplied by the Nernst Equation for the non-standard concentrations (in this case $V_{\text{Nernst}} = 0.0592 \log[\text{H}^+] \text{ V} = -0.844 \text{ V}$), and the potential drop across the Calomel reference electrode ($V_{\text{CRE}} = (0.2415 \text{ V})$).

$$\eta_c (\text{V}) = V_{\text{cathode}} - (E_{\text{cell}}^0 + V_{\text{Nernst}} + V_{\text{CRE}})$$

$$\eta_c (\text{V}) = V_{\text{cathode}} - 0.0 \text{ V} - 0.844 \text{ V} + 0.2415 \text{ V}$$

A plot of the measured current density, as a function of the over voltage for four different cathode materials: Pt wire, 100 nm diameter RuO₂ NRs on Ti, blanket RuO₂ thin film on Ti, and Ti metal foil, is shown in Figure 7.

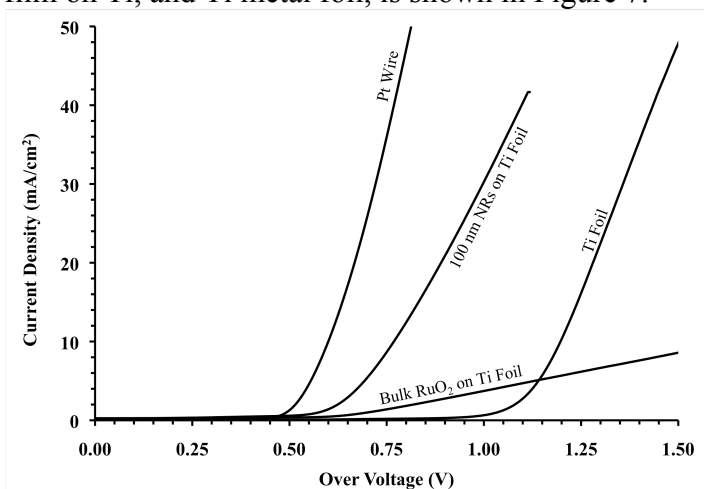


Figure 7. Electrical characterization of various cathode constructed of Pt wire, 100 nm diameter RuO₂ NRs on Ti, blanket RuO₂ thin film on Ti, and Ti metal foil. A

10% aqueous KOH solution was used as the electrolyte and a Pt wire was used as the anode.

Two of the curves shown in Fig. 6 result from a Ti substrate that is covered with some form of RuO_2 , a continuous thin film of RuO_2 and a film of uniformly distributed RuO_2 nanorods. The chemical and/or galvanometric behavior of these two cathodes is expected to be identical. It was incorrectly assumed at the beginning of this investigation that a high electrical field could be generated at the sharp corners and pyramid shaped caps of the RuO_2 nanorods and would modify the electrical potential near the surface of the nanorods resulting in a change in the chemical reactivity of the electro-catalyst for H_2 production. To verify this, the above results for the two RuO_2/Ti electrodes were normalized and compared for equal interfacial areas in contact with the aqueous solution reactant.

To investigate this effect, the interfacial area corrected current density for the four different electrode systems shown in Fig. 6. were re-plotted in Fig. 8. The interfacial area correction term is determined by adding the total surface area of the individual nanorods and the flat substrate surface per unit area of the Ti substrate electrode surface. It is interesting to observe that the interfacial area corrected current density for the two RuO_2 coated cathodes, i.e. the bulk RuO_2 thin film and nanorod coated substrates in Fig. 7, have merged in Fig. 8. This result suggests that the reason for the increase in the performance of the nanorod coated electrode over the blanket thin film coated electrode is explained as the increased interfacial contact area with the solution afforded by the nanorods.

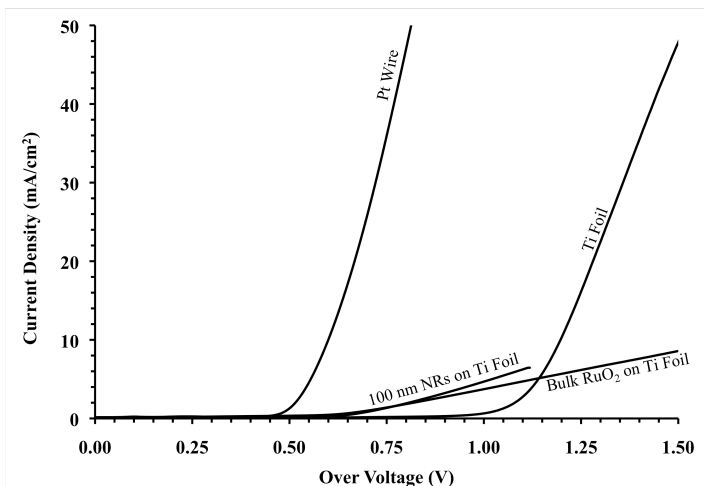


Figure 8. Electrical characterization of RuO_2 nanorods grown on Ti foil substrates. A 10% KOH solution was used as the electrolyte and a Pt wire used as the anode. The area contribution of the nanorods has been taken into consideration.

The large difference in performance for the three electrode materials shown in Fig. 8 is dependent on the electro-chemical nature of the electrode material i.e. Pt, RuO_2 , and Ti and not the geometric shape of the cathode surface. These results show that an increased activity expected with the increase in the electrical field at the edges of the nanorods has not been obtained. In a dielectric fluid such as water, and less so in an

aqueous ionic solution, a double layer (DL) is formed on the surface of the electrode. This surface charge then creates an electrostatic field that terminates on oppositely charged ionic species in the dielectric fluid. The thickness of this DL, Debye Layer, is expected to be in the range of a few nanometers, and will be uniformly distributed across any surface which comes in contact with the dielectric liquid. The formation of a fringing electrical field at the corners and peak of the nanorods will not occur. The potential drop across the DL is predicted by Gouy-Chapman Theory which is well known in the field of electrochemistry of the solid-liquid interface.

The minimum voltage theoretically required to split a water molecule is given by the expression $\frac{\Delta G^0}{nF}$ where $\Delta G^0 = 237.2$ KJ/mole (at STP), n = number of electrons transferred, F = Faraday's Constant, and $V_{cell}^{min} = 1.23$ V. The actual operating voltage required in a practical experiment however is defined as;

$$V_{opt} = -\frac{\Delta G^0}{nF} + IR + \Sigma\eta$$

Where the last two terms in the above expression are the Ohmic drop across the solution and the sum of the over potentials required to initiate the splitting of water in an electrolyzer. The summation of over potentials includes components due to the non-standard electrolyte concentration, transport of charges across the interfacial layer surrounding the electrodes, and the chemical activation of the chemical reaction occurring at the electrode surfaces. The over potential resulting from non-standard electrolyte concentrations is given by the Nernst correction (V_{Nernst}) and was discussed above. The only significant component of the over potential summation, for the low current regime used herein, is expected to be due to the chemical activation at the electrode surface.

To further understand the performance of the nanorod electrolyzer system, the variation between the different electrode materials is considered. As discussed above, the only other significant component of the summation of over potentials is that due to the chemical activation of the reaction occurring at the electrode surface. Therefore, the vertical axis can be labeled either as the activation potential or operating voltage, see Figure 9. The activation potentials plotted for current densities greater than 10 mA/cm^2 , coincides with the generation of bubbles due to water splitting and not leakage.

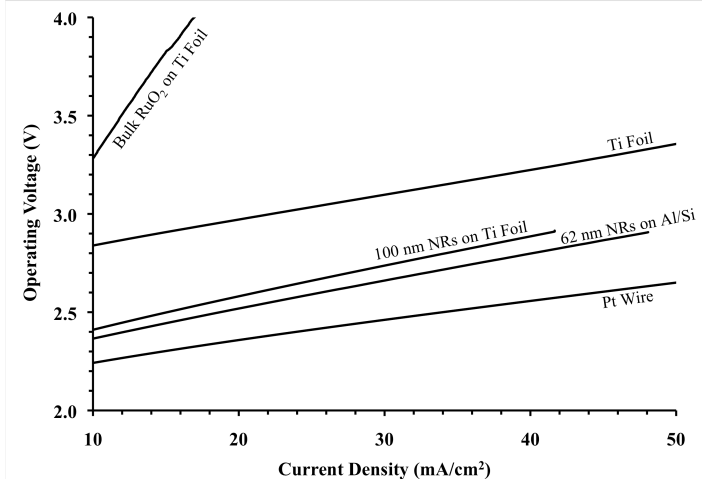


Figure 9: Over voltage or activation potential versus current density for electrolysis performed with a 10% aqueous solution of KOH.

Assuming that an energy of 1.23 eV can be stored from the electrolysis of one molecule of water, the above data has been used to calculate the efficiency expected from the conversion of electrical power to H₂ as a fuel, see Figure 10.

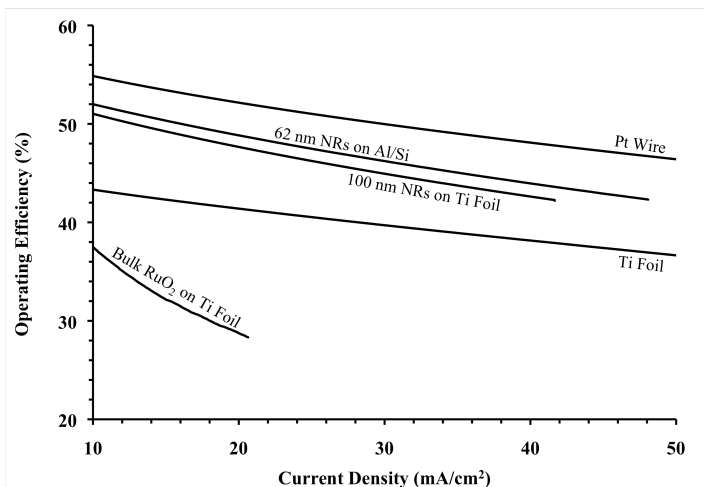


Figure 10: Operating Efficiency vs Current Density. 10% KOH solution was used.

The fact remains that Pt is the best material to use as the cathode for the electrolysis of water. The use of the RuO₂ nanorods as the electro-catalyst material on the cathode is approximately 2.5 % less efficient and considering future improvements or an increase in the cost of P, may result in a reconsideration of what is the best choice in materials..

The effect of the nanorod covered cathode surface on the efficiency to produce hydrogen by electrolysis of an aqueous KOH solution was found to be solely dependent on the electrode's increased interfacial contact area with the liquid. There was no increase in activity that resulted from the shape of the nanorods, which might be caused by a high electric field in the vicinity of the nanorods. The results were explained by the formation of a double layer adjacent to the electrode surface, whose interfacial area increased with the nanorod cathodes. The results were ultimately used to calculate the efficiency expected from an electrolyser constructed of the different cathode materials.

4. Pt film or Pt containing quantum dots dramatically affects the hydrogen producing ability of RuO₂ Nanorods

Our laboratory was able to grow RuO₂ nanorods decorated with Pt quantum dots (See Figure 11).

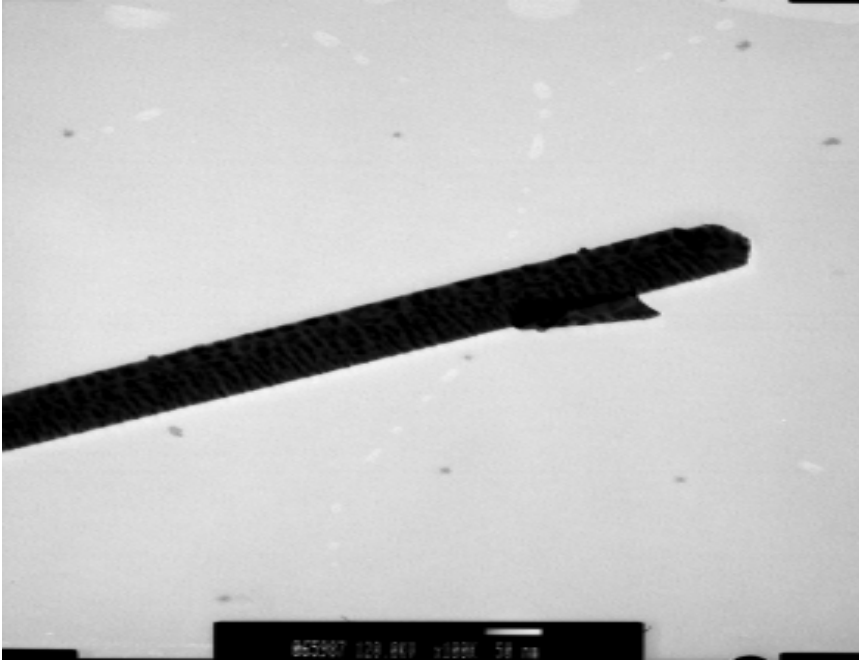


Figure 11. SEM image of a RuO₂ nanorod, decorated with Pt quantum dots.

An unanticipated downside to the increased catalytic abilities of these Pt decorated nanorods was their increased corrosion in air, at an elevated temperature of only 300 C. On the positive side the production of hydrogen was drastically affected as can be seen in Figure 10 below. It is feared however if these materials are to be used as long lasting permanent electrode in a hydrogen production facility, they will be in need of replacement after a short period of time making them uneconomical. It was apparent that our system needed to be modified, with one thought being that the nanorods needed to be completely coated by the Pt additive, to prevent the oxidation of the RuO₂ nanorod.

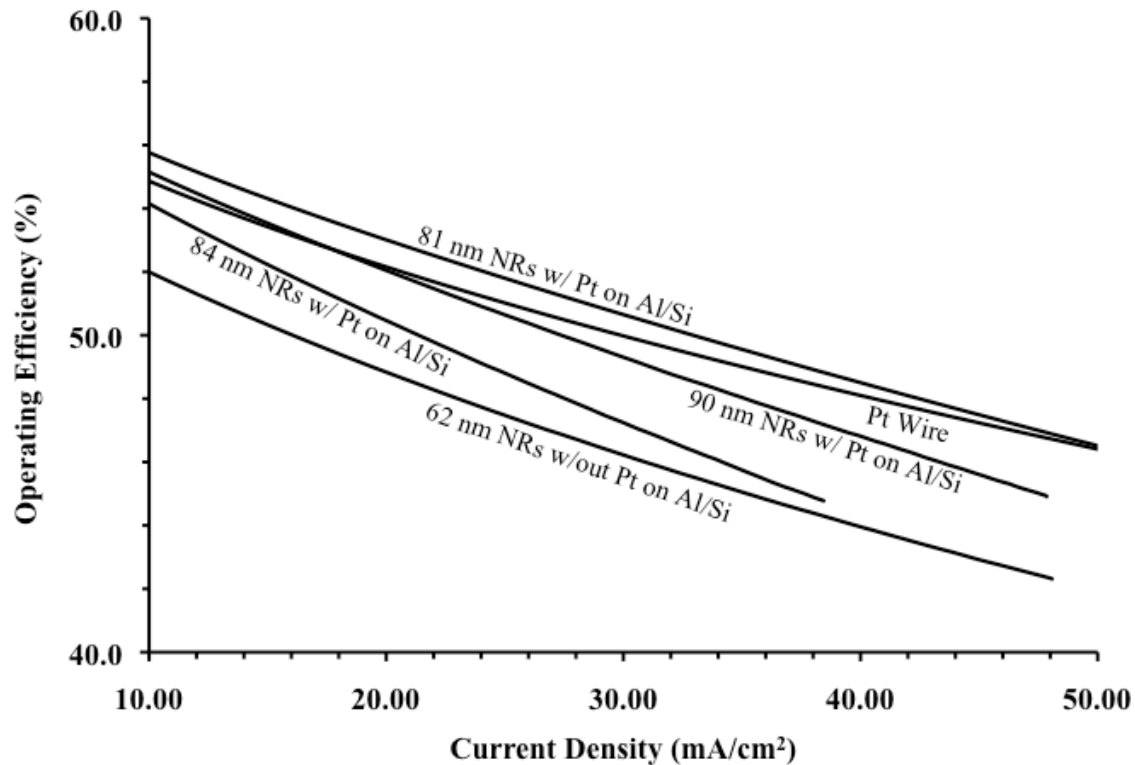


Figure 12. Hydrogen production by electrolysis with the RuO₂ nanorod coated cathode electrode.

Investigation by Yves Dubief

Inflow and Outflow BC with Dissipative Particle Dynamics

(Progress Report)

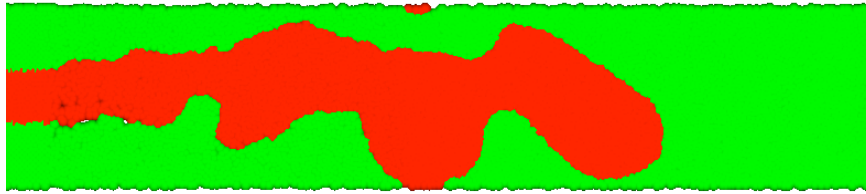
Presently our efforts have focused on representation of non-periodic boundary conditions such as inflow and outflow boundary conditions in dissipative particle dynamics code we have been working on. Recent advances in the treatment of walls have demonstrated the applicability of DPD to nano and microchannels, however some basic issues remain such as the definition of adequate inflow and outflow boundary conditions, as most simulations have, so far, used periodic and wall boundary conditions. Most of the practical engineering flows are with non-periodic boundary conditions. In reality very few flows are with periodic boundary conditions. Finally a droplet formation is achieved with the inflow and outflow boundary conditions based on conservation of mass and conservation of thermodynamic properties to simulate spatially developing flows using DPD.

We have successfully implemented wall boundary conditions, where particles are made stuck to their initial positions using spring force. Right now we are in the process of implementing inflows and outflows in a channel in x-direction. The droplet formation is

observed in a channel by simulating two immiscible fluids with the help of DPD with right parameters as shown in the figure below.

Presently code is being changed to sort out the compressibility issues, which will help keeping the density constant through out the flow. Future work will be comprised of implementing inflow and outflow boundary conditions in y and z directions too.

The domain was discretized on a Cartesian uniform grid composed of squares or cubes of volume $v = r_a^{n_d}$, where n_d is the dimension of the simulation. The code discretizes the domain in cubes of length equal to the cutoff of the conservative potential. The discretization has two objectives. First it speeds up the computation of particle-particle interaction in the case of inflow and outflow boundary conditions compared to the generation of Verlet lists. Second, it allows the treatment of boundary conditions using the continuum arguments and it is designed as an interface to a future coupling with a computational fluid dynamics code. At each time step, the solution of the particle field is computed at cell center locations. The continuum solution at each cell center includes the velocity vector for each specie, temperature T and pressure P of the flow.



(a) Flow of two immiscible fluids in a channel with open BC forming droplet.

Non-Periodic Boundary Conditions

A. Walls

Since most developments of molecular dynamics algorithms have been targeted at systems that can easily accommodate periodic boundary conditions, little attention has been paid to non-periodic boundary conditions with the exception of walls. In implementing solid-liquid interfaces in DPD simulations, the difficulty arises in modeling macroscopic boundary conditions such as no slip at impenetrable interfaces like walls. Hence, in order to avoid spurious behavior at the walls such as particle layering, temperature variations or artificial slip, forces exerted on, the liquid at the walls must be matched carefully. In this work, we used a solid boundary model, which represents the solid by an amorphous, thermally rough configuration of particles, resulting in a thin diffuse sl -interface.

The conservative force law in DPD acts on particles at sl -interface, i.e., the walls, the same way it acts on all other particles depending on the local environment. Initially DPD was implemented on all liquid particles for 2000 iterations to reach equilibrium. Then the solid-liquid system was constructed by dividing the entire equilibrated slab of thickness L_y in the y-direction into two boundary regions (walls) of thickness $2r_c$ and inner (liquid) region of thickness $L_y - 2r_c$. The positions of sl -interfaces were marked by $y_{int} = \pm(L/2 - 2r_c)$. Inflow-outflow boundary conditions were applied in the x-direction.

To make the boundary regions into walls, at some time t_0 after reaching equilibrium, each particle i at position $\mathbf{r}_i(t_0) = (x_i(t_0), y_i(t_0))$ with $|y_i(t_0)| > |y_{int}|$ is permanently fixed to the

position $\mathbf{r}_i(t_0)$ by implementing the spring force $\mathbf{F}_s = -k_s (\mathbf{r}_i(t) - \mathbf{r}_i(t_0))$. The interactions of particles in the walls are maintained with right values of parameters without causing spurious behavior at the sl -interface. A diffuse interface of thickness $d = 0.25r_c$ was created so that, for $|y| > |y_{\text{int}} \pm d|$, $\mathbf{F}_{\text{ext}} = -B (y - (y_{\text{int}} \pm d))$ acts on liquid particles only to prevent indefinite diffusion into the walls.

B. Inflow

In many microfluidic applications, the emptying of syringes at a control rate creates flows. The first priority for simulations is therefore the ability to prescribe mass fluxes at the inlets, which may be accomplished in several manners.

Particle injection: This simple method consists of injecting one or more particles at a fixed time increment determined by the prescribed inlet mass flux at the inlet surface. The location of injected particles may be random or lattice-based. This method has the disadvantage to create a particle field that is not equilibrated in the vicinity of the inlet.

Equilibrated coupled inflow: To eliminate the drawback of the particle injection method, the inlet is coupled with an independent DPD simulation. The simulation is periodic in the direction of the flow, which is driven by an external force. The external force may fluctuate in time to impose constant mass flux. At each time step, particles that cross a given plane of the inflow simulation are injected in the spatial simulation.

Inflow boundary conditions need to prescribe given mass fluxes. The injection of particles at a constant rate seems an obvious strategy. The problem is to develop a strategy for the choice of the initial position of injected particles that does not create out-of-equilibrium state. For instance, randomly seeding the inlet boundary may result, at times, in the formation of a cluster of particles. The repulsive nature of the conservative particle-particle interaction for small distances is then likely to create unrealistically large velocities. Thus different strategies are implemented to minimize and/or eliminate the risk.

C. Outflow

Depending on the problem at hand, one may wish to fix several variables at the outlets of a computational domain v . We considered the most restrictive case, where pressure, temperature are expected to be statistically constant at the boundary and density is statistically constant over v . The governing equation for density is the conservation of mass:

$$\int_v \frac{\partial \rho}{\partial t} dV + \int_{\partial v} \rho (\mathbf{v} \cdot \mathbf{n}) dS = 0$$

The first term in the above equation is effectively the temporal derivative of the mass of all the particles contained in the system $\partial M(t)/\partial t$. Let $\dot{M}_{\text{in}}(t)$ and $\dot{M}_{\text{out}}(t)$ be the mass fluxes at the inlet and outlet surfaces of the domain. The inlet mass flux, for example, is estimated on the Eulerian grid:

$$\dot{M}_{\text{in}}(t) = \sum_{i \in \partial V_e^{\text{in}}} \left\langle \sum_{j \in V_e^{\text{in}}(x_i^e)} \rho_j (\mathbf{V}_j \cdot \mathbf{n}_i) \right\rangle_{(x_i^e, t)} \Delta S_e$$

If the simulation is fully incompressible, the temporal variation of the mass is null. In practice, the mass varies and its temporal derivative may be written as a harmonic oscillator designed to let the mass fluctuates around a target value M_* . As a first approach, we propose to control the mass inside the domain by correcting the velocity in the cells

that map the outlet surface of the Eulerian grid. The velocity correction is uniform to simplify its calculation:

$$v_{out}(t) = \frac{1}{M_{\partial V_{out}}} \left[\dot{m}_{out}(t) - \dot{m}_{in}(t) - \frac{1}{\tau_M} (M_{\infty} - M(t)) \right]$$

where $M_{\partial V_{out}}$ is the mass of all particles contained in exit unit cells. The impedance time of total mass oscillator is defined as τ_M . For $\tau_M = \Delta t$, the oscillator is effectively the mass derivative of a system whose mass increases or decreases to recover the targeted mass over one time-step. This velocity correction method is compact in its determination, via the mass of the system, but local in its application, as only the particles in unit cells crossing the Eulerian outlet boundary are affected. This aspect is particularly important for the period of injecting particles in a vacuum. This may work well in channels where surface tension may be able to hold particles forming the edge of the fluid to stray. In most configurations, however it is more likely that an atomization of atoms may occur, leading to large variations of density fluctuations. The velocity correction may then halt or even reverse the trajectory of particles due to the mass oscillator. A second approach to initialization is to start from an equilibrated spatial distribution of particles with zero mean momentum. Lastly, a third method uses a continuum velocity field for the configuration of interest to initialize velocity of all particles in the domain. Under such conditions, the initial correction velocity is initially zero and is less likely to develop oscillations in the system. Unfortunately, such a field may not always be available.